Stability of the C_NH_i complex and the BL2 luminescence band in GaN

M. A. Reshchikov,[1] O. Andrieiev,[1] M. Vorobiov,[1] B. McEwen,[2] F. Shahedipour-Sandvik,[2] D. Ye,[1] and D. O. Demchenko,[1]

[1] *Department of Physics, Virginia Commonwealth University, Richmond, VA 23220, USA*

[2] *College of Nanoscale Science and Engineering, SUNY Polytechnic Institute, Albany NY, USA*

Abstract

The dissociation of the C_NH_i complex in GaN is studied in detail by using photoluminescence measurements and first principles calculations. The BL2 band with a maximum at 3.0 eV is caused by electron transitions from an excited state located at 0.02 eV below the conduction band to the ground state of the C_NH_i donor with the 0/+ level 0.15 eV above the valence band. The dissociation releases hydrogen atom, and the remaining C_N defect with the –/0 state at 0.92 eV above the valence band is responsible for the YL1 band with a maximum at about 2.2 eV. The dissociation of the C_NH_i complex can be caused by the photo-induced defect reaction mechanism under UV illumination at low temperatures (~20 K), leading to the bleaching of the BL2 band and simultaneous rise of the YL1 band. The bleaching is reversible. Alternatively, the complex dissociates after annealing at temperatures above 600 °C. The activation energy of this process (3-4 eV, depending on the annealing geometry) corresponds to the removal of hydrogen from the sample and not to the dissociation of the complex itself.

I. INTRODUCTION

Point defects in GaN affect the properties of the material and the performance of GaN-based devices. Photoluminescence (PL) is an efficient, non-destructive tool in studying point defects in semiconductors,[1] yet still, the assignments of several PL bands in GaN are lacking or unreliable. First-principles calculations help identify the defects associated with particular PL bands, and in return accurate experimental results provide unique information for validation of theoretical methods. In this study, we systematically investigated the carbon-hydrogen complex (C_NH_i) in GaN by using the combination of experimental and theoretical methods.

A blue luminescence (BL) band with a maximum at 2.9-3.0 eV is often observed in PL spectra from GaN, especially from layers grown by metalorganic chemical vapor deposition (MOCVD) technique.[1] In undoped *n*-type GaN samples, the BL band with a maximum at 2.9 eV and the zero-phonon line (ZPL) at 3.10 eV (labeled BL1) appear due to contamination of GaN with Zn during growth. The BL1 band is caused by transitions via the Zn_{Ga} acceptor with the $-/0$ level at 0.40 eV above the valence band. In other samples (usually highly resistive), a similar BL band (labeled BL2) appears with a maximum at about 3.0 eV and the ZPL at 3.33 eV. The characteristic feature of the BL2 band is its gradual disappearance under UV illumination at low temperatures, known as the PL bleaching. The BL2 bleaching is accompanied by the rise of the yellow band with a maximum at 2.2 eV (the YL1 band).[1] We proposed earlier that the C_NH_i complex may be the origin of the BL2 band in GaN, and dissociation of this complex under UV light produces isolated C_N defects responsible for the YL1 band.[2,3]

Recent reports further clarify the origin of BL2 band in GaN. Wu *et al*.[4] demonstrated that annealing at 1000 °C for 1 hour of semi-insulating GaN grown by MOCVD results in the

disappearance of the BL2 band and an increase of the YL1 band. These results supported the hypothesis that the C_NH_i complex and isolated C_N cause the BL2 and YL1 bands. The reduction of the H concentration below the detection limit after the annealing was directly confirmed by secondary ion mass spectrometry (SIMS) measurements. By repeating annealing at temperatures from 600 to 1000 °C with an increment of 100 °C, the authors of that paper observed that the BL2 band disappears between 600 and 800 °C and estimated the activation energy of the complex decomposition as 2.3-2.5 eV. The dissociation of the C_NH_i complexes in Mg-doped GaN grown by MOCVD after annealing at 700 °C in nitrogen ambient was also observed from analysis of infrared absorption peaks attributed to vibrational modes of this complex.[5]

The dissociation of the H-containing complexes in GaN and the diffusion of hydrogen in *n*- and *p*-type GaN attracted significant attention in the past.[6] The most studied case of dissociation of H-containing complexes in GaN is the behavior of Mg-doped GaN grown by MOCVD. Nakamura *et al*.[7] demonstrated that after thermal annealing in an N_2 ambient at temperatures above 700 °C, the resistivity of GaN:Mg grown by MOCVD decreased by a factor of 5×10^5. After annealing in NH_3 ambient at $T > 600$ °C, the high resistivity was restored.[8] Similarly, the introduction of H_2 into MBE-grown GaN:Mg substantially reduces the concentration of free holes.[9] The high resistivity of as-grown GaN:Mg and its significant reduction after annealing were attributed to the formation of the Mg-H complexes in GaN grown by MOCVD and their dissociation at $T > 600$ °C.[7,8,9,10,11,12] Diffusion of hydrogen in GaN strongly depends on its conductivity type. While in *p*-type GaN, hydrogen diffuses readily at $T > 600$ °C, no diffusion could be observed in *n*-type GaN up to 1020 °C.[11,13]

Early first-principles calculations predicted that the barrier for diffusion of the H^+ ions in the *c* direction is 0.94 eV and that for the H^- ions is 1.99 eV.[14] More recent calculations using the generalized gradient approximation of Perdew-Burke-Ernzerhof (GGA PBE) and Heyd-Scuseria-Ernzerhof (HSE) hybrid functional methods revealed that the HSE barrier for diffusion of the H^+ diffusion along the *c* axis is 1.08 eV, and the barrier for the dissociation of the $Mg_{Ga}H_i$ complex is 1.88 eV.[15]

In addition to the complex dissociation and H^+ diffusion barriers, there is a barrier for hydrogen to leave a GaN sample. Myers *et al*.[16] estimated the activation energy for recombinative desorption of hydrogen to be at least 2 eV. The results of that work show that the release of hydrogen is limited by a surface permeation barrier, not by dissociation or diffusion.

In this work, we aim to understand the details of the C_NH_i complex dissociation and its effect on PL by using the latest first-principles calculations approach, annealing of samples under different conditions, and detailed analysis of PL.

II. THEORY

A. First-principles calculations

Theoretical calculations were performed using the HSE hybrid functional,[17] tuned to fulfill the generalized Koopmans condition for carbon acceptor C_N in GaN (the fraction of exact exchange of 0.25, the range separation parameter of 0.161 $Å^{-1}$).[18] Calculations were performed in 300-atom hexagonal supercells at the **Γ**-point, with plane-wave energy cutoffs of 500 eV. Defect formation energies were computed following an established procedure.[19] All atoms were relaxed within HSE to minimize forces to 0.05 eV/Å or less. Spurious electrostatic interactions in calculated total energies were corrected using the Freysoldt-Neugebauer-Van de Walle approach.[20,21]

Adiabatic potentials used to plot the configuration coordinate diagrams were obtained by fitting into HSE computed energies using harmonic approximation. The diffusion barriers for the dissociation of hydrogen from the carbon-hydrogen complex were calculated using the nudged elastic band method with the above HSE parametrization in 128-atom hexagonal supercells. Elemental chemical potentials used in defect formation energy calculations were obtained from the total energies of the GaN growth competing phases. For example, in a Ga-rich growth regime, the chemical potential of nitrogen is set to $\mu_{\mathrm{N}}(\mathrm{N}_2)+\Delta H_f(\mathrm{GaN})$, while that of gallium is set to $\mu_{\mathrm{Ga}}(\mathrm{Ga\ metal})$, where ΔH_f(GaN) is the formation enthalpy of GaN. In the presence of nitrogen, the chemical potential of hydrogen is assumed to be limited by the formation of ammonia NH_3.

Figure 1 shows the formation energies of the C_NH_i complex and its constituents, isolated C_N and H_i defects, computed assuming Ga-rich growth conditions, which favors the formation of N-substituting defects, such as C_N and C_NH_i. Hydrogen interstitial has several sites in GaN lattice with similar formation energies.[2] Among these, the lowest energy site for Fermi energies, E_F, below about 3 eV is the bond-center site, where a positively charged hydrogen is located in the middle of the Ga-N bond along the wurtzite c-axis, labeled $BC_{||}$ site. Positively charged hydrogen occupying the antibonding nitrogen (AB_N) site has very similar formation energies to that of the $BC_{||}$ site. For $E_F > 3$ eV, the lowest energy configuration of interstitial hydrogen is the antibonding Ga site (AB_{Ga}) in a singly negative charge state. Interstitial hydrogen is forming a negative-U defect with the calculated value of U of about −0.25 eV, changing its geometry from $BC_{||}$ or AB_N in the positive charge state to the AB_{Ga} in the negative charge state. The energies of the neutral hydrogen in $BC_{||}$ or AB_N sites are also similar. Notable differences in values of the formation energies shown in Fig. 1 and those in Ref. 2 stem from the differences in choices of

the elemental chemical potentials. Also, larger values of U were reported previously for hydrogen interstitial, i.e. -0.77 eV in Ref. 2 as obtained using bandgap tuned HSE, and -2.4 eV as obtained by local approximations to the density functional theory.[22]

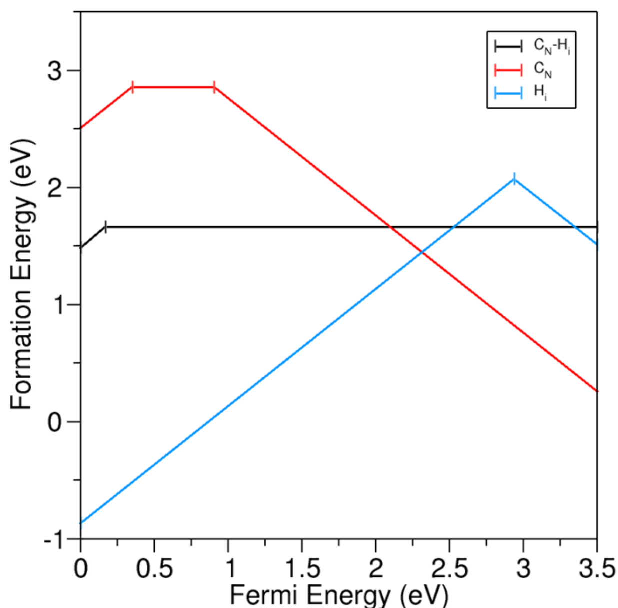

Fig. 1. Formation energies of the C_N, C_NH_i, and H_i defects as a function of the Fermi energy in the GaN bandgap, calculated for Ga-rich conditions.

The C_N acceptor has been extensively discussed before as a source of the yellow PL band (YL1) associated with the 0/- acceptor level at 0.916 eV above the valence band maximum (VBM).[3,23,24] In addition, the C_N also forms a deep donor +/0 level at about 0.3 eV above the VBM, responsible for the BL_C band with a PL maximum at 2.9 eV, which appears in *n*-type GaN only at high excitation intensities, after all 0/- levels are saturated with holes.[3, 25,26,27] The HSE calculations show that Coulomb attraction between negative C_N and positive H_i leads to forming a stable C_NH_i complex, which is a deep donor with a calculated +/0 transition level at 0.18 eV. In its lowest energy configuration, the interstitial hydrogen occupies an antibonding carbon (AB_C) site (see inset to Fig. 2). Hydrogen at a C-Ga bond center site has formation energy that is about

0.5 eV higher. Bader charge analysis,[28] based on HSE computed charge densities along the hydrogen removal path (shown in Fig. 2), suggests that a neutral C_NH_i complex dissociates into a negative C_N acceptor and a positively charged interstitial hydrogen H_i, regardless of the Fermi energy. Therefore, the calculated binding energy of the C_NH_i complex, defined as the energy difference between the neutral C_NH_i complex and its oppositely charged isolated constituents, is 1.3 eV, suggesting a stable complex.

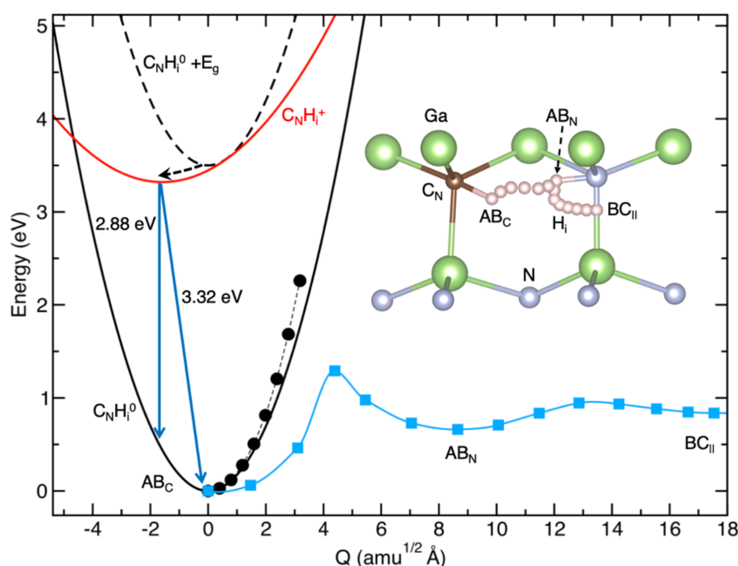

Fig. 2. Configuration coordinate diagram and calculated optical transitions for the C_NH_i complex. Filled circles show direct HSE calculation of the $C_NH_i^0$ adiabatic potential. Filled squares show energy along the diffusion path as a function of configuration coordinate Q. The HSE calculated diffusion pathway with hydrogen moving from the AB_C site to the $BC_{||}$ site is also illustrated.

The HSE calculations suggest that optical transitions via the +/0 transition level of the C_NH_i complex form the BL2 band. Figure 2 shows the configuration coordinate diagram of this defect. In the dark, the complex is in a neutral charge state (Fig. 1), shown as a lower adiabatic potential $C_NH_i^0$ in Fig. 2. A photogenerated electron-hole pair raises the energy of the system by the energy of the bandgap (3.5 eV), shown with an upper dashed adiabatic potential labeled

$C_NH_i^0+E_g$. The photogenerated hole is captured nonradiatively (dashed arrow) at the +/0 transition level at 0.18 eV above the VBM with no barrier for the capture, transferring the defect into the positive charge state shown as an upper adiabatic potential labeled $C_NH_i^+$. The path for a nonradiative transition to the ground state involves a barrier of about 0.5 eV; i.e., the intersection of the + and 0 adiabatic potentials. This suggests that the low-temperature transitions via the +/0 transition level are predominantly radiative. The nonradiative transition barrier of 0.5 eV is higher than the energy of 0.18 eV needed to thermally eject the hole into the valence band. This also suggests that the C_NH_i complex remains radiative before thermal quenching of the BL2 band occurs. The subsequent radiative recombination of the localized hole with a free electron leads to the BL2 band with the calculated ZPL at 3.32 eV and the PL maximum at 2.88 eV, in good agreement with the experiment.

Figure 2 also demonstrates the experimentally observed photo-bleaching of the BL2 band. The removal of hydrogen along the lowest energy diffusion path was calculated using the nudged elastic band method with HSE hybrid functional for a neutral C_NH_i complex. Starting with hydrogen occupying the AB_C site, H_i moves towards the AB_N site and subsequently to the lowest energy $BC_{\|}$ site. As shown in Fig. 2, the computed dissociation energy barrier of the C_NH_i complex is 1.3 eV (unrelated to the complex binding energy of the same value). The transitions forming the lower energy side of the BL2 band, which leave the C_NH_i complex in a highly strained state, provide the relaxation energy sufficient for the complex dissociation following the optical transition with the energies roughly below 2 eV (i.e., the energy of the ZPL minus the energy of the complex dissociation barrier). However, the direction of configuration coordinate Q for the effective vibrational mode of the neutral C_NH_i complex is sufficiently different from the direction of the lowest energy dissociation path. The energies along these two configuration

directions are compared in Fig. 2 as filled circles and filled squares. The direct HSE calculations in the direction of Q immediately following the optical transition (filled circles) show continuously increasing energies that are significantly larger than those in the direction of the lowest energy dissociation path (filled squares). This suggests that the photobleaching of the BL2 band is significantly less efficient than what could be expected from the calculated complex dissociation barrier of 1.3 eV and lattice relaxation energies. Furthermore, the lowest energy dissociation path is not a straight line in a multidimensional space of configuration coordinates. This path can be followed as a result of diffusion rather than lattice relaxation following the optical transition in the effective vibrational mode of the defect. Therefore, the dissociation of the C_NH_i complex due to the excess of the lattice relaxation energy following the optical transition could happen in a weaker vibrational mode, which would promote the hydrogen in the direction of the lowest energy dissociation path. This is indeed observed in the experiment (see Sec. IVC), where photo-bleaching dissociation is estimated to occur only for every 10^7-th transition with energy below 1.4 eV. Upon dissociation, the barrier for the diffusion of the interstitial hydrogen is relatively low (0.3 eV). However, at low temperatures for which the PL measurements are performed (about 20 K), this value suggests limited diffusion, and that the hydrogen is located close to the next nearest neighbor site of the C_N acceptor following the photo-induced complex dissociation. As shown in Fig. 2, in the vicinity of the C_N acceptor, the energy of interstitial hydrogen increases by 0.66 eV in the AB_N site and by 0.84 eV in the $BC_{\|}$ site. These values are lower than the complex binding energy of 1.3 eV (which assumes infinite separation of C_N and H_i) due to the long-range Coulomb interaction between C_N^- and H_i^+. The barrier for the complex restoration is about 0.65 eV, suggesting the possible BL2 restoration in samples at room temperature.

In the experiment, the BL2 band can also be quenched as a result of annealing. The 0.3 eV barrier for the diffusion of the interstitial hydrogen indicates that it easily moves in the GaN lattice, even below room temperature. The dissociation barrier of 1.3 eV suggests that C_NH_i complex is dissociated at about 500 K. At the same time, a relatively low restoration barrier of 0.6 eV suggests that the Coulomb interaction can also lead to the complex restoration at room temperatures. This means that unless the hydrogen out-diffuses as a result of annealing, the dissociated complexes can restore during the sample cooling or over several days at room temperature.

B. Phenomenological model

By using the Shockley-Reed-Hall approach to analyze rate equations in application to PL in semiconductors,[29,30] we construct a model and write rate equations for GaN with four recombination channels. The radiative recombination includes three PL bands: the YL1, BL2, and near-band-edge (NBE) emission, labeled with indexes 1, 2, and 3, respectively, and the nonradiative recombination channel represented by the most efficient nonradiative defect labeled *S* (Fig. 3).

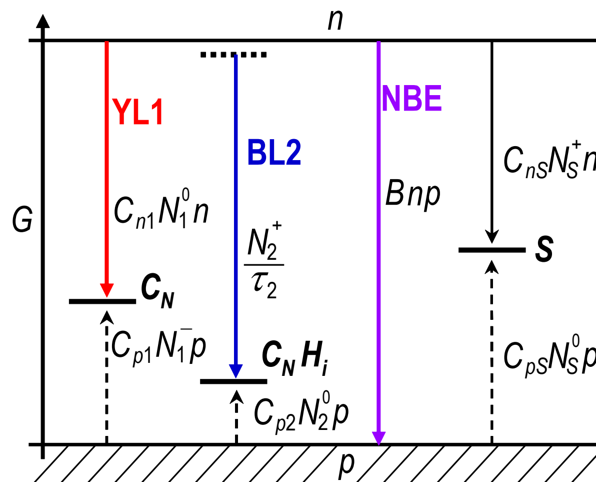

Fig. 3. The band diagram accounting for three types of defects (C_N, C_NH_i, and the nonradiative center *S*) and the NBE emission. The solid and dashed arrows show transitions for electrons and holes, respectively.

The studied samples are *n*-type so that all the defect levels in the gap below shallow donors are filled with electrons in the dark. For low excitation intensities (below the saturation of defects with photogenerated charge carriers), the concentrations of holes bound to the defects are small and can be ignored compared to the total concentrations. Then, the rate equation for free holes in the valence band in steady-state conditions is

$$G = \frac{p}{\tau_p} = C_{p1} N_1 p + C_{p2} N_2 p + Bnp + C_{pS} N_S p \, , \tag{1}$$

where

$$\tau_p = \left(C_{p1} N_1 + C_{p2} N_2 + Bn + C_{pS} N_S \right)^{-1} . \tag{2}$$

Here G (cm^{-3}s^{-1}) is the electron-hole generation rate, p and n are the concentrations of free holes and electrons, τ_p is the characteristic lifetime of holes in the valence band, and the terms on the right side of Eq. (1) are the hole-capture rates by the corresponding four recombination mechanisms: via the C_N acceptors with the concentration N_1 and hole-capture coefficient C_{p1}, the C_NH_i donors with corresponding parameters N_2 and C_{p2}, the NBE channel with the effective capture coefficient B, and the nonradiative recombination channel with effective parameters N_S and C_{pS}.

The dissociation of the C_NH_i complex due to extended illumination at low temperatures or annealing at high temperatures results in isolated C_N defects. The total concentration of the

carbon-related defects remains constant: $N_{C_N} = N_1 + N_2$. The quantum efficiencies of the three radiative recombination channels are $\eta_1 = \tau_p C_{p1} N_1$, $\eta_2 = \tau_p C_{p2} N_2$, and $\eta_3 = \tau_p B n$. We will describe the dissociation of the C_NH_i complex with a function D, which is equal to 1 in an as-grown sample and decreases according to a specific dissociation mechanism. Then, in general,

$$N_1 = N_{10} + N_{20}(1 - D_i) \tag{3}$$

and

$$N_2 = N_{20} D_i , \tag{4}$$

where N_{10} and N_{20} are the concentrations of the C_N and C_NH_i defects in the as-grown sample, respectively, and the index i indicates the dissociation mechanism: $i = a$ for the annealing at high temperatures, and $i = b$ for the bleaching at low temperatures. The expressions for D_i for the two cases are derived below.

With increasing temperature, the C_NH_i complexes dissociate with the probability

$$w = t_{ann} \nu \exp\left(-\frac{E_1}{kT_{ann}} \right), \tag{5}$$

where t_{ann} is the time of annealing at temperature T_{ann}, ν is the dissociation attempt frequency (can be taken as the phonon frequency, about 10^{13} s^{-1}), and E_1 is the activation energy of the dissociation. Note, however, that the barrier for the hydrogen diffusion in bulk GaN and the barrier for the thermal removal of H from the surface may be the limiting factors in the removal of H. We expect that the concentration of C_NH_i complexes decreases with annealing as [31,32,33,34]

$$N_2 = N_{20} D_a = N_{20} \exp\left[-t_{ann} \nu \exp\left(-\frac{E_a}{kT_{ann}} \right) \right], \tag{6}$$

and the concentration of the isolated C_N defects increases as

$$N_1 = N_{10} + N_{20}\left(1 - D_a\right). \tag{7}$$

Here, D_a is the probability of converting a C_NH_i complex to an isolated C_N defect after annealing, and E_a is the effective activation energy, which in general may include dissociation, migration, and hydrogen out-diffusion barriers. Note that the PL measurements are conducted at low temperatures, and the complexes may form again during the cooling process unless hydrogen is removed from the sample.

In PL experiments at low temperatures, we observe the bleaching of the BL2 band simultaneously with the rise of the YL1 band. This phenomenon can be explained by the dissociation of the C_NH_i complexes.[2] The rate of transitions via the C_NH_i complexes in steady-state conditions is $\eta_2 G$. The radiative recombination rate for a given C_NH_i center is $\eta_2 G / N_2$. If the fraction of recombinations leading to the dissociation of the C_NH_i complex is γ, and it is much smaller than the radiative recombination rate, then the rate of the complex dissociations is

$$\lambda = \frac{\eta_2 G \gamma}{N_2}. \tag{8}$$

In the first approximation (neglecting the reverse process), the concentration of the C_NH_i complexes is expected to decrease with the time of laser exposure as

$$N_2(t) = N_{20} D_b = N_{20} \exp\left(-\lambda t\right), \tag{9}$$

where D_b is the BL2 bleaching function.

From Eqs. (1)-(4), we can find the quantum efficiencies η_i of the radiative recombination channels accounting for the dissociation of the C_NH_i complexes:

$$\eta_{BL2} \equiv \eta_2 = \eta_{20} \frac{\tau_p}{\tau_{p0}} D_i \,, \tag{10}$$

$$\eta_{YL1} \equiv \eta_1 = \eta_{10} \frac{\tau_p}{\tau_{p0}} \left[1 + \frac{N_{20}}{N_{10}} (1 - D_i) \right], \tag{11}$$

$$\eta_{NBE} \equiv \eta_3 = \eta_{30} \frac{\tau_p}{\tau_{p0}} \,, \tag{12}$$

where $\frac{\tau_p}{\tau_{p0}} = \left[1 + \eta_{20} \left(\frac{C_{p1}}{C_{p2}} - 1 \right) (1 - D_i) \right]^{-1}$, and the dissociation function D_i is given by Eq. (6) for annealing and Eq. (9) for bleaching.

Analysis of the BL2 band bleaching dynamics and the YL1 band rise with laser exposure allows us to determine the hole-capture coefficient for the C_NH_i defect when such coefficient for the C_N acceptor is known. Indeed, the concentration of the C_NH_i complexes changes by $-\Delta N$, and the concentration of the C_N defects increases by the same amount. Then, the intensities of the YL1 and BL2 bands change by $\Delta \eta_1 = \tau_p C_{p1} \Delta N$ and $\Delta \eta_2 = -\tau_p C_{p2} \Delta N$, respectively. By defining the ratio R of these changes as $R = -\Delta \eta_2 / \Delta \eta_1$, we find that

$$C_{p2} = -C_{p1} \frac{\Delta \eta_2}{\Delta \eta_1} = R C_{p1} \,. \tag{13}$$

Thus, from quantitative analysis of the BL2 bleaching and the YL1 rise, the C_{p2} can be determined. In principle, the C_{p2} can also be found from the analysis of the BL2 and YL1 intensities after annealing. However, as will be shown below, the latter method is less reliable.

III. EXPERIMENTAL DETAILS

Nominally undoped GaN layers with a thickness of 3.5-3.8 μm were grown on sapphire substrate by MOCVD. Two 2-inch wafers (s1564 and s1587) were cut into 5×5 mm samples for detailed study. Low-temperature PL measurements confirmed the uniformity of properties in these samples. From the SIMS measurements, the C, H, O impurities concentrations in sample s1587 are ~1.7×10^{17}, ~3.0×10^{17}, and ~1.3×10^{17} cm^{-3}, respectively. The concentration of Si was below the SIMS detection limit (<10^{16} cm^{-3}) in similar samples. From the Hall-effect measurements, the samples are *n*-type with moderate conductivity. In particular, sample s1587 has the concentration of free electrons $n = 2.6\times10^{16}$ cm^{-3} and the electron mobility $\mu_n = 400$ cm^2/Vs at room-temperature. Note that only some carbon impurities exist as the C_N acceptors, while the C_NH_i complexes, being deep donors, are inactive in electrical measurements. Assuming that the total concentration of shallow donors (O_N and Si_{Ga}) is $N_D = 1.4\times10^{17}$ cm^{-3} and their effective ionization energy is 20-30 meV, we obtain that the total concentration of acceptors is 1.05×10^{17} cm^{-3}. This value agrees with the estimates of the C_N concentration from PL and SIMS (Sec. IIIF).

For annealing experiments, selected samples were annealed at SUNY in N_2 ambient under the pressure of 1 atm for one hour and temperatures from 300 to 800 °C. The ramp rate was ~100 °C/min. After the anneal, no changes were observed in the measurements of the Hall effect, SIMS, or AFM for any sample. At VCU, three types of annealing were explored. The first type is nearly identical to SUNY's annealing procedure using a single-zone quartz tube furnace. The samples were loaded at the center of the quartz tube. The quartz tube was first evacuated to pressure around 1 Torr by a vacuum pump and then flushed with N_2 gas three times before raising the N_2 pressure to slightly above 1 atm. Once the N_2 flow was stabilized around 15 sccm, the annealing procedure started. The heating ramp rate was 20 °C/min. At target temperature,

annealing was conducted for one hour. In the second type, the annealed sample was covered with another GaN layer on a sapphire substrate (the face-to-face configuration). In these experiments, the annealing temperature range was increased to 1100 °C. In the third type, N_2+H_2 ambient was used instead of pure nitrogen. In this type, the quartz tube was evacuated and flushed with N_2 and then introduced H_2 and N_2 gases as the annealing environment. The H_2 gas flow was kept fixed at 5 sccm while N_2 was at about 15 sccm to maintain the pressure inside the tube to be slightly above 1 atm. The samples were annealed at 850 °C for one hour.

Steady-state PL was excited with a HeCd laser with the power density P_{exc} = 0.13 W/cm^2. The laser power was attenuated with neutral-density filters to achieve lower excitation intensities, and the laser beam was focused with a lens to achieve higher P_{exc}. The measured PL spectrum was corrected for the spectral response of the measurement system and multiplied by λ^3 (where λ is the PL wavelength) to present the spectra as the number of emitted photons as a function of photon energy $\hbar\omega$. The absolute internal quantum efficiency for each PL band was estimated by comparing the integrated intensities of these bands with the ones in calibrated GaN samples. All the measurements were conducted in identical conditions. Other details can be found in Ref. 1.

IV. RESULTS AND DISCUSSION

A. Photoluminescence spectrum

PL spectra from GaN samples before and after annealing were analyzed in detail, including the bleaching effect and the restoration process. In this section, selected PL spectra are analyzed to support the attribution of the studied PL bands and tabulate their parameters. Figures 4-6 show

low-temperature PL spectra from as-grown GaN and after annealing at 1050 °C. The NBE emission consists of the donor-bound-exciton (DBE) peak at 3.480 eV, the free exciton (FE) peak at 3.488 eV, followed by two longitudinal optical (LO) phonon replicas, and the $n = 2$ state of the FE line at 3.513 eV (the inset to Fig. 5). The details of the NBE spectra can be better resolved at high P_{exc}. From positions of the DBE and FE lines, and assuming the binding energy of the FE to be 25 meV,[35] the bandgap energy (E_g) in the studied sample was calculated as E_g = 3.513 eV, blue-shifted by 10 meV from the value in thick, unstrained GaN.[35]

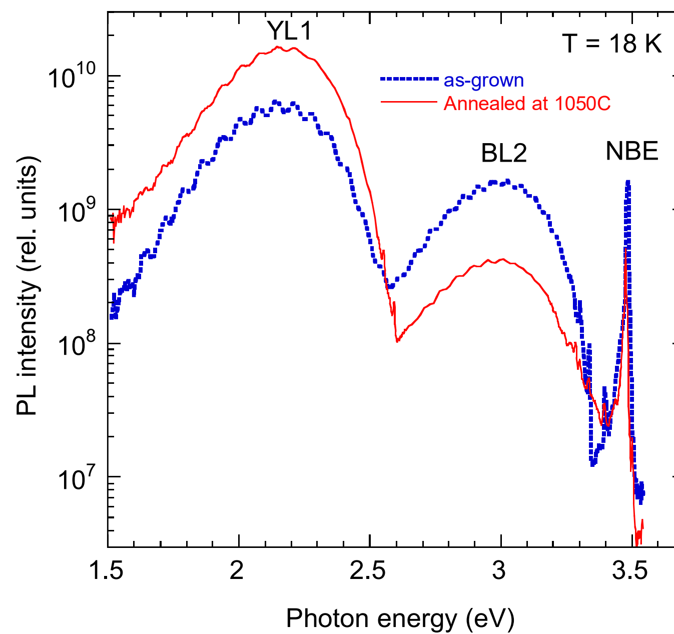

Fig. 4. PL spectra at T = 18 K and P_{exc} = 10^{-4} W/cm^2 before and after annealing at 1050 °C (in the face-to-face geometry). The oscillations (with separations between maxima of ~0.07 eV) are caused by Fabry-Pérot interference in the 3.8 µm-thick GaN layer.

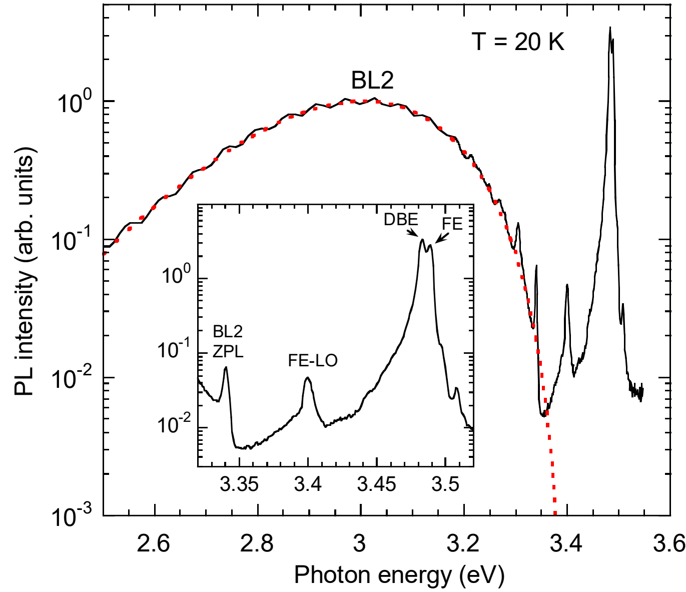

Fig. 5. The BL2 and NBE bands in as-grown GaN. P_{exc} = 0.16 W/cm^2. The dashed line is calculated using Eq. (14) with the following parameters: S_e = 4.6, d_{FC}^{g} = 0.38 eV, E_0^* = 3.38 eV, Δ = 0.005 eV. The inset zooms in the high-energy part.

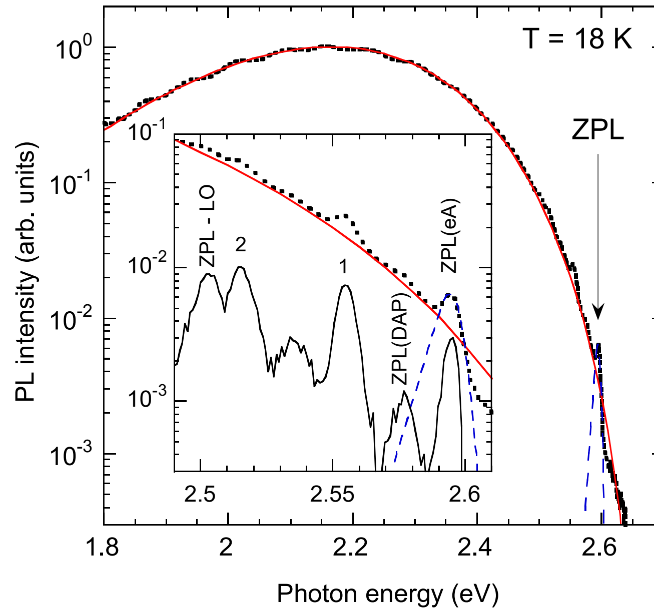

Fig. 6. The YL1 band in GaN (sample s1587) annealed at 1050 °C (face-to-face). The BL2 band is subtracted. The solid red line is calculated using Eq. (14) with the following parameters: S_e = 7.3, d_{FC}^{g} = 0.50 eV, E_0^* = 2.66 eV, Δ = 0.005. The inset shows the high-energy part of the YL1 band and the fine structure obtained after subtracting the smooth component described with Eq. (14). 1 and 2 are pseudo-local phonon replicas with energy 40 meV.

The main defect-related PL bands are the YL1 band with a maximum at 2.2 eV and the BL2 band at 3.0 eV. The shapes of these broad bands were fitted with the following expression obtained in the one-dimensional configuration-coordinate model [36]

$$I^{PL}(\hbar \qquad \hbar \qquad \left[-2S_e\left(\sqrt{\frac{E_0^*-\hbar}{d_{FC}^g}} \qquad 1\right)^2\right]. \tag{14}$$

Here, S_e is the Huang-Rhys factor in the excited state of the defect, $d_{FC}^g = E_0^* - \hbar$ is the Frank-Condon shift in the ground state, $E_0^* = E_0 + 0.5\hbar$, E_0 is the ZPL energy, $\hbar$ is the energy of the effective phonon mode in the excited state, $\hbar$ and $\hbar$ are the photon energy and position of the PL band maximum, respectively. The Δ is the PL band shift due to sample-dependent reasons such as in-plane biaxial strain in thin GaN layers grown on sapphire substrates.

The YL1 and BL2 bands have been recognized by their positions, shapes, ZPLs, and characteristic phonon-related fine structure. The ZPL was observed at 2.595 eV for the YL1 band and at 3.340 eV for the BL2 band. In a sample with low intensity of the BL2 band (decreased due to annealing at 1050 °C and additional exposure to laser for several hours), a weak ultraviolet luminescence (UVL) band was observed with the ZPL at 3.290 eV. The ZPLs of the three PL bands did not shift (with the uncertainty of ±0.2 meV) with a variation of P_{exc} by several orders of magnitude. After careful analysis of the behavior of the ZPL and phonon-related fine structure with temperature and excitation intensity, we concluded that the ZPLs of the YL1 and UVL bands are caused by electron transitions from the conduction band to the

acceptors with the ionization energies 918 and 224 meV, respectively. The bands are attributed to the C_N and Mg_{Ga} defects. [3,24,37]

The BL2 band is attributed to transitions from an excited state of the C_NH_i complex located at about 20 meV below the conduction band to the ground state located at 0.15 eV above the valence band. The excited state's position was estimated from analysis of the BL2 spectra at different temperatures in a C-doped, semi-insulating GaN sample with a lower NBE emission contribution (Fig. 7).

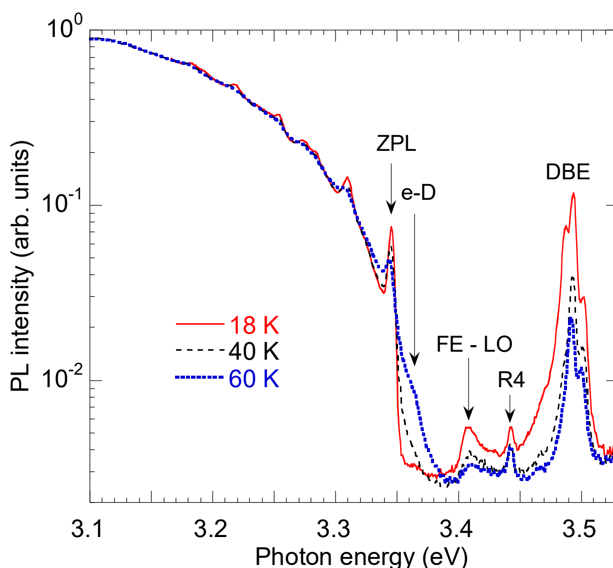

Fig. 7. Evolution of the high-energy side of the BL2 band in MOCVD GaN:C sample (MD9856) with the temperature at P_{exc} = 0.02 W/cm^2. The shoulder labeled e-D is attributed to electron transitions from the conduction band to the ground state of the C_NH_i donor.

Since the C_NH_i defect is a deep donor, an excited hydrogenic state may appear close to the conduction band when it captures a hole. In *n*-type GaN, with the Fermi level close to the conduction band, the C_NH_i defects are neutral. Thus, a photogenerated hole must be captured first. Then a free electron is quickly captured by the excited state. Finally, an internal transition

from the excited to the ground state causes the BL2 band. This transition's characteristic time equals the PL lifetime measured in time-resolved PL experiments ($\tau_2 \approx 300$ ns). The exponential decay of the BL2 band (and its ZPL) after a laser pulse, even at the lowest temperature (18 K) and the same PL lifetime in different samples (including semi-insulating and weakly conductive) support the assumption on the internal transition. With increasing temperature, transitions from the conduction band contribute to the BL2 band as evidenced by a shoulder at high-energy side of the ZPL at $T \approx 60$ K (Fig. 7).

B. Thermal quenching of photoluminescence

With increasing temperature, the BL2 intensity starts decreasing above ~50 K (Fig. 8).

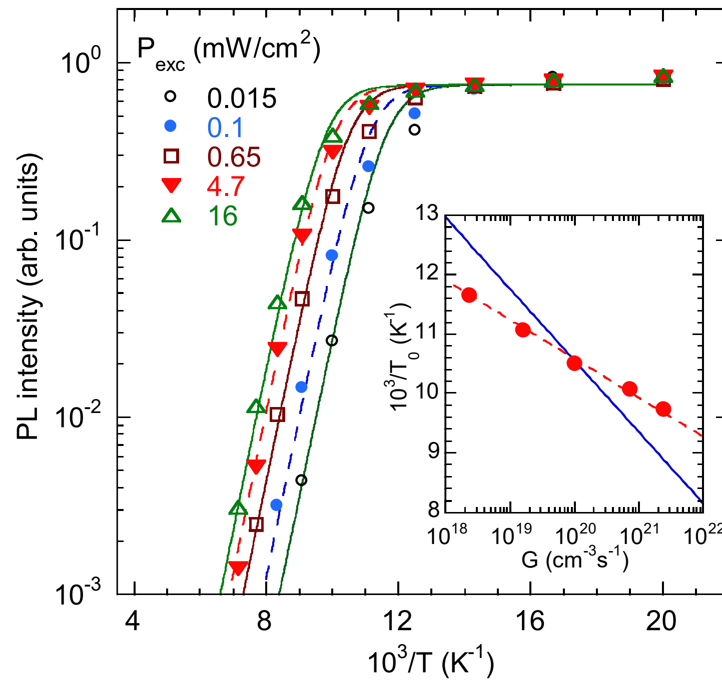

Fig. 8. Temperature dependence of the BL2 intensity (normalized at $T = 30$ K) at selected P_{exc}. The lines are calculated using Eqs. (15) and (16). The inset shows the dependence of the critical temperature T_0 on G.

The $I^{PL}(T)$ dependence is usually described by the following expression [35]

$$I^{PL}(T) = \frac{I^{PL}(0)}{1 + C\exp\left(-\frac{E_A}{kT}\right)}, \tag{15}$$

where C is a constant and E_A is the activation energy. According to the Schön-Klasens mechanism of PL quenching, typical for defects in n-type GaN,[29,30,38]

$$C = \left(1-\eta_0\right)\tau_0 C_p N_v / g\ . \tag{16}$$

Here, C_p and g are the hole-capture coefficient and degeneracy of the defect, respectively, η_0 and τ_0 are the absolute internal quantum efficiency (IQE) and lifetime of PL at temperatures before the quenching begins, and N_v is the effective density of states in the valence band. The activation energy as obtained by fitting to the data shown in Fig. 8 (E_A = 165 meV) is very close to the distance from the C_NH_i level to the valence band (expected to be 0.15 eV from the position of the BL2 band's ZPL). However, the parameter C is inversely proportional to P_{exc}; i.e., the quenching is tunable by the excitation intensity,[30] and attempts to use Eq. (16) lead to unreasonably large values (up to $C_p = 10^{-2}$ cm^3/s).

The tunable and abrupt quenching of PL is explained by a sudden transition from a nonequilibrium condition (often with population inversion) to a quasi-equilibrium condition at a characteristic temperature T_0 increasing with excitation intensity.[30,38] This mechanism of PL quenching is common for semi-insulating materials.[38] The $T_0(P_{exc})$ or $T_0(G)$ dependence reveals

the ionization energy E_i of the defect from which holes are emitted to the valence band and restore the equilibrium condition: [30]

$$T_0 = -\frac{E_i}{k \ln\left(G/B\right)} \tag{17}$$

with

$$B = C_p \left(\frac{1}{\eta_0} - 1\right)(N_A - N_D)\frac{N_v}{g}, \tag{18}$$

where N_D and N_A are the concentrations of shallow donors and defects responsible for the PL quenching (in our case, the $C_N H_i$), respectively.

Two fits of the experimental $T_0(G)$ dependence are shown in the inset to Fig. 8. The best fit (dashed line) reveals unreasonable parameters (E_i = 300 meV and $B = 10^{36}$ cm^{-3}s^{-1}). Indeed, with $\eta_0 \approx 0.1$, $N_A - N_D \approx 10^{17}$ cm^{-3}, and $N_v/g \approx 10^{18}$ cm^{-3}, we obtain $C_p \approx 1$ cm^3/s. However, by fixing E_i = 165 meV, we find a less perfect fit (the solid line) but reasonable B and C_p values (6×10^{28} cm^{-3}s^{-1} and ~10^{-7} cm^3/s, respectively). This departure of the fit with reasonable parameters from the experimental dependence can be explained qualitatively by the surface effect, which is not accounted for in the simple model. The depletion region and electric field may be significant even under above-bandgap illumination at T = 20-100 K.[1] Unblocking of the nonradiative channel will occur at higher temperatures than T_0 because the electric field sweeps holes to the surface. Moreover, the quenching region will stretch in temperature because the band bending and the depletion region width increases with increasing temperature.

Interestingly, the Hall effect measurements indicate that the studied GaN samples are not semi-insulating but n-type with the room-temperature concentration of free electrons $n = 2\times10^{16}$

cm^{-3}. PL data also indicate that the samples are *n*-type. In particular, the YL1 decay is nearly exponential at room temperature ($\tau \approx 50$ μs), and the DBE line increases linearly with P_{exc} at T = 20 K.

When PL quenching occurs with the tunable mechanism, the $I^{PL}(T)$ dependence can formally be fitted with Eq. (15), yet the coefficient C (and also C_p in Eq. (16)) becomes ridiculously large.[30,38] For *deep* acceptors, the parameter E_A becomes abnormally large and lacks physical meaning: the PL intensity simply drops at $T \approx T_0$. After the drop, the PL intensity is nearly temperature-independent (if the sample is *p*-type) or decreases with the slope equal to the defect's ionization energy (if the sample is high-resistivity *n*-type). Interestingly, for defects with low ionization energy, the magnitude of the abrupt drop is small so that the activation energy of the quenching is close to the ionization energy.[38] In this case, the $I^{PL}(T)$ dependence can be explained with Eq. (15), in which $C = B/G$.[1] The quenching of the BL2 band occurs by this mechanism.

C. Bleaching of the BL1 band

From the analysis of the BL2 bleaching and the YL1 rise in about 20 samples, including undoped and C-doped GaN grown by MOCVD and hydride vapor phase epitaxy (HVPE) methods, we obtained $R = -\Delta\eta_2 / \Delta\eta_1$ = 0.12±0.02. Note that only relative quantum efficiencies or relative integrated PL intensities for the BL2 and YL1 bands are needed for this estimate. Then, by using Eq. (13) and C_{p1} =(3.7±1.6)×10^{-7} cm^3/s for the YL1 band,[39] the value of C_{p2} = (4.4±2.0)×10^{-8} cm^3/s is found for the capture of holes by the C_NH_i complex. We emphasize that in the process of

the BL2 bleaching, the total number of the C_N-containing defects is conserved, while the total intensity of the YL1 and BL2 bands changes due to different values of C_p for these two defects.

Examples of the evolution of the YL1, BL2, and NBE quantum efficiencies with the time of exposure with the HeCd laser are shown in Figs. 9 and 10. The dependences in Fig. 10 are fitted using Eqs. (8)-(11) with the only fitting parameter γ (other parameters, estimated in Sec. IVF, play a minor role). As the P_{exc} increases by a factor of 10^3, the BL2 bleaching rate increases by about the same amount (Fig. 10). The obtained value of $\gamma = 5\times10^{-8}$ indicates that only one out of 10^7-10^8 electron-hole recombinations via the C_NH_i complex leads to the dissociation, in agreement with earlier estimates.[40] We suggest that only electron transitions with energy $\hbar\omega < E_{cr} = E_0 - E_B$ can cause the dissociation of this complex after emitting a photon (Fig. 2).

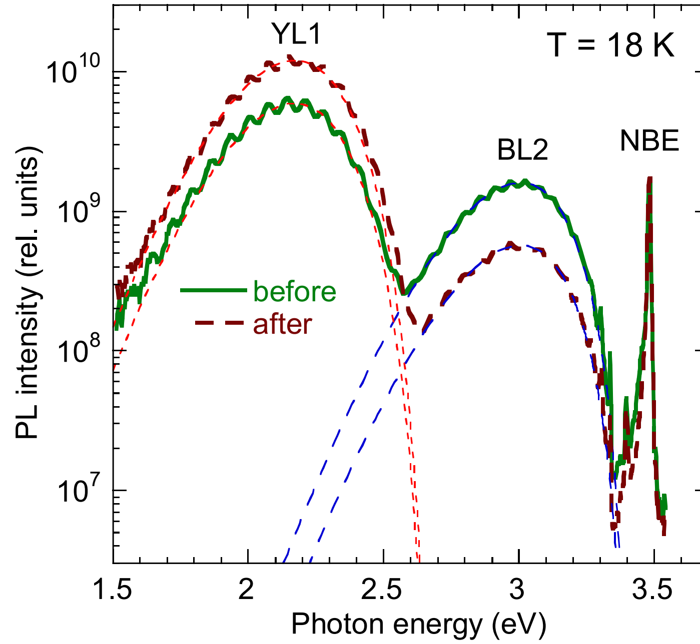

Fig. 9. PL spectrum from as-grown GaN (sample s1587) measured at T = 18 K and P_{exc} = 10^{-4} W/cm^2 before and after exposure with P_{exc} = 0.13 W/cm^2 for 80 min. The thin dashed lines are calculated using Eq. (14) with the following parameters: S_e = 7.5, d^g_{FC} = 0.50 eV, E^*_0 = 2.66 eV, Δ = 0.01, $I^{PL}(\hbar\omega_{max}) = 0.6\times10^{10}$ (before) and 1.2×10^{10} (after) for the YL1 band and

$S_e = 4.6$, $d_{FC}^{g} = 0.38$ eV, $E_0^* = 3.0$ eV, $\Delta = 0.005$, $I^{PL}(\hbar\omega_{\max}) = 1.6 \times 10^9$ (before) and 0.58×10^9 (after) for the BL2 band.

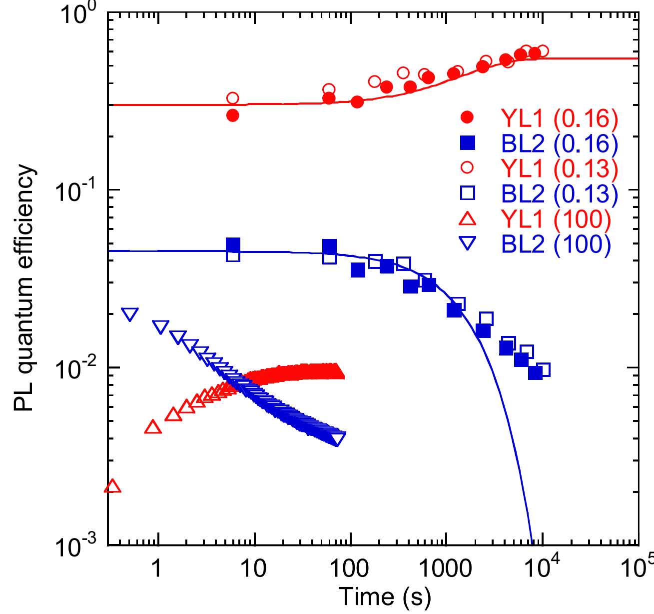

Fig. 10. Evolution of PL quantum efficiency for the YL1 and BL2 bands in as-grown GaN (sample s1587) with the time of exposure with the HeCd laser with $P_{exc} = 0.13$, 0.16 and 100 W/cm^2 at $T = 18$ K. The lines are calculated using Eqs. (8)-(11) with the following parameters: $\gamma = 5\times10^{-8}$, $\eta_1 = 0.3$, $\eta_2 = 0.05$, $N_{10} = 7\times10^{16}$ cm^{-3}, $N_{20} = 1\times10^{17}$ cm^{-3}, $R = 0.12$. The bleaching of the BL2 band and concurrent rise of the YL1 band at $P_{exc} = 100$ W/cm^2 occurs at about 10^3 times shorter time scale.

The fraction of these transitions can be found as the ratio of the BL2 intensity integrated between $\hbar\omega = 0$ and $\hbar\omega = E_{cr}$ to the total integrated intensity of this band. From Eq. (13) describing the shape of the BL2 band, we find that $\gamma = 5\times10^{-8}$ corresponds to $E_{cr} = 1.4$ eV; i.e., the effective barrier for the dissociation is 1.9 eV. Note that from first-principles calculations we obtained $E_B = 1.3$ eV for the lowest-energy dissociation barrier (Sec. IIA). The discrepancy can be explained by the fact that the theoretically calculated dissociation barrier $E_B = 1.3$ eV is located in a direction that is substantially different from the direction of defect relaxation following the optical transition.

D. Annealing of GaN

The Arrhenius plots for several annealing experiments are shown in Fig. 11. For two samples annealed at SUNY, the BL2 intensity abruptly decreases between 600 and 675 °C. For one of these samples (s1587) annealed at VCU, the abrupt drop of the BL2 intensity begins at slightly higher temperatures (by about 60 °C). The difference could be attributed to the specifics of the setups and slightly different annealing conditions (ramping rate, nitrogen pressure). Interestingly, when the GaN sample surface was covered by another undoped GaN sample (the face-to-face annealing geometry), the BL2 decrease began at much higher temperatures (above 1000 °C), suggesting that the out-diffusion of hydrogen from the sample causes this decrease, rather than dissociation of the C_NH_i complex. The latter process is likely reversed during the sample cooling.

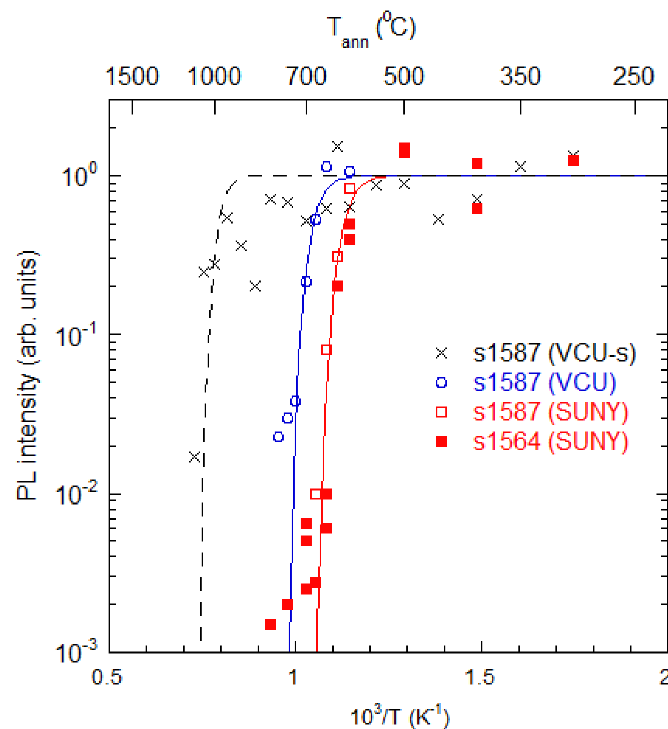

Fig. 11. Dependence of the BL2 intensity on the annealing temperature. The lines are calculated using Eqs. (6) and (10) with the following parameters (from left to right): E_a = 4.2 eV, 3.18, and 2.95 eV.

The annealing temperature dependences for the BL2 band were fitted with Eqs. (6) and (10) with the only fitting parameter E_a (Fig. 11). For uncovered GaN sample, $E_a \approx 3.0$ eV, while for the sample covered with another GaN piece, $E_a \approx 4.2$ eV. Examples of PL spectra before and after face-to-face annealing are shown in Fig. 4. The expected from Eq. (11) increase of the YL1 and NBE intensities after annealing at high temperatures is small and could not be reliably confirmed in the experiments. The YL1 intensity uncontrollably increased or decreased by up to half an order of magnitude after annealing at a particular temperature. Other factors, such as the formation or dissapearance of nonradiative defects or the surface changes, probably affect these PL bands more significantly than the dissociation of the C_NH_i complexes. For this reason, the values of R and C_{p2} cannot be reliably found from the annealing experiments. However, the BL2 intensity decreases by orders of magnitude above a critical annealing temperature (Fig. 11), so that the activation energy for the process leading to its decrease is determined fairly accurately.

E. Restoration of the BL2 band

After exposing GaN samples to HeCd laser light at P_{exc} = 0.13 W/cm^2 for one hour at T = 18 K, the BL2 intensity decreased by ΔI_{BL2}, and the YL1 intensity increased by ΔI_{YL1}, with $\Delta I_{BL2}/\Delta I_{YL1}$ = $R \approx$ 0.1-0.2 (Sec. IVC). Then the temperature was raised to 300 K, and the sample was kept in the dark for 15 hours. After that, the sample was cooled down to 18 K in the dark, and PL measurements were conducted at very low P_{exc} to avoid the saturation of the PL bands and bleaching during the experiment. After this cycle, the original spectra were partially restored.

Such experiments were repeated multiple times, both with as-grown and annealed samples. The intensity of the YL1 band was restored by (0.6±0.2)ΔI_{YL1}, and that of the BL2 band by (0.6±0.3)ΔI_{BL2}. After keeping the sample for only 0.5-1 hour at T = 300 K following prolonged low-temperature bleaching, the restoration of PL intensities was insignificant (by about 10%).

In Sec. IIA, we attributed the PL restoration to hydrogen moving from one of the near local potential minima (Fig. 2) back to the global minimum, thereby re-forming the C_NH_i complex. To find the probability of the C_NH_i complexes restoration at room temperature after the low-temperature BL2 bleaching, Eq. (5) can be used, in which T_{ann} = 300 K and E_1 in this case is the barrier for the complex restoration (Fig. 2). The experimental results indicate that $E_1 \approx 1.0$ eV, not much different from the value predicted by theory (0.65 eV). On the other hand, the PL from GaN samples annealed at high temperatures was measured again after prolonged storage of the samples at room temperature (for more than two months). No significant changes were observed, which indicates that the annealing caused the removal of hydrogen from the sample.

To find whether the C_NH_i complexes can be restored by hydrogenation, we annealed samples in H_2+N_2 ambient at 850 °C for 1 hour. Figure 12 shows a PL spectrum of as-grown GaN after annealing in the N_2 ambient and after the subsequent annealing at 850 °C in the H_2+N_2 ambient. After the first annealing (in N_2), the BL2 band disappeared (its intensity decreased by at least three orders of magnitude). After the subsequent hydrogenation, the BL2 intensity was restored to almost the initial intensity (Fig. 12). The intensities of all bands slightly decreased after this cycle, likely due to the formation of some nonradiative defects.

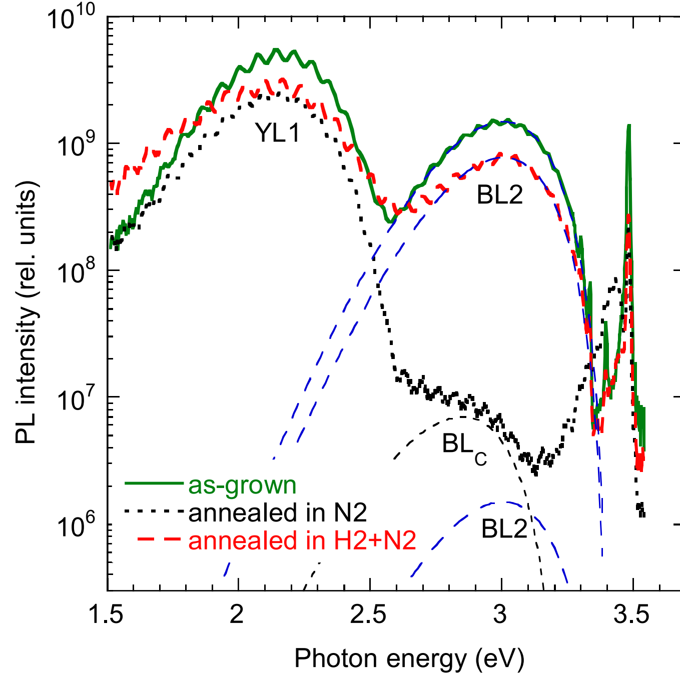

Fig. 12. PL spectra of GaN (sample s1587) at $T = 18$ K and $P_{exc} = 10^{-4}$ W/cm^2. After annealing in N_2 at 850 °C for 1 hour, the BL2 intensity decreased by at least a factor of 1000. After additional annealing in H_2+N_2 at 850 °C, the BL2 band was almost completely restored. The shape of the BL2 band is calculated using Eq. (14) with parameters given in Fig. 5. The BLc band with the maximum at 2.8 eV is caused by electron transitions from the conduction band to the 0/+ level of the C_N defect.[3]

F. Concentrations of defects contributing to photoluminescence spectrum

The concentrations of defects contributing to PL can be estimated from PL intensity dependence on excitation intensity.[39,41] The PL intensity or IQE for the i-th type of defect depends on photon flux P as

$$\frac{I_i^{PL}(P)}{I_{i0}^{PL}} = \frac{\eta_i(P)}{\eta_{i0}} = \frac{P_i^{cr}}{P} \ln\left(1 + \frac{P}{P_i^{cr}}\right), \tag{19}$$

where the critical excitation intensity at which saturation of PL begins is

$$P_i^{cr} = \frac{N_i}{\eta_{i0}\alpha\tau_i^{\lim}} . \tag{20}$$

Here, N_i is the concentration of the related defect, $\tau_i^{\lim}$ is the longest time in the recombination process (usually, $\tau_i^{\lim}$ is the PL lifetime τ_{i0}), η_{i0} and I_{i0}^{PL} are the IQE and PL intensity in the limit of low excitation intensity, and α is the absorption coefficient for GaN at 3.8 eV. When the concentration of one type of defect is found or known, the concentrations of defects responsible for other PL bands can be found by comparing their integrated PL intensities and knowing the hole-capture coefficients. [1,29,39]

$$\frac{N_i}{N_j} = \frac{C_{pj}}{C_{pi}} \frac{I_i^{PL}}{I_j^{PL}} . \tag{21}$$

The excitation intensity dependences were analyzed for as-grown GaN and GaN annealed at 1050 °C in face-to-face geometry (Fig. 13). For the as-grown sample, the measurements were done with a short laser exposure for high excitation intensities to avoid the bleaching-related drift. On the other hand, the annealed sample was exposed to P_{exc} = 100 W/cm^2 for an hour to achieve the lowest contribution of the BL2 band before taking the $I^{PL}(P_{exc})$ dependence. Note that the BL2 band still could be observed in the latter case, yet with larger uncertainty (see error bars in Fig. 13) because it overlapped with the C_N-related BL_C band with a maximum at 2.85 eV. By fitting the excitation intensity dependences for the BL2 band with Eq. (19), we have estimated that $N_{BL2} \approx 5\times10^{16}$ cm^{-3} in the as-grown sample and $N_{BL2} \approx 5\times10^{14}$ cm^{-3} in GaN annealed at 1050 C° (after one hour of bleaching).

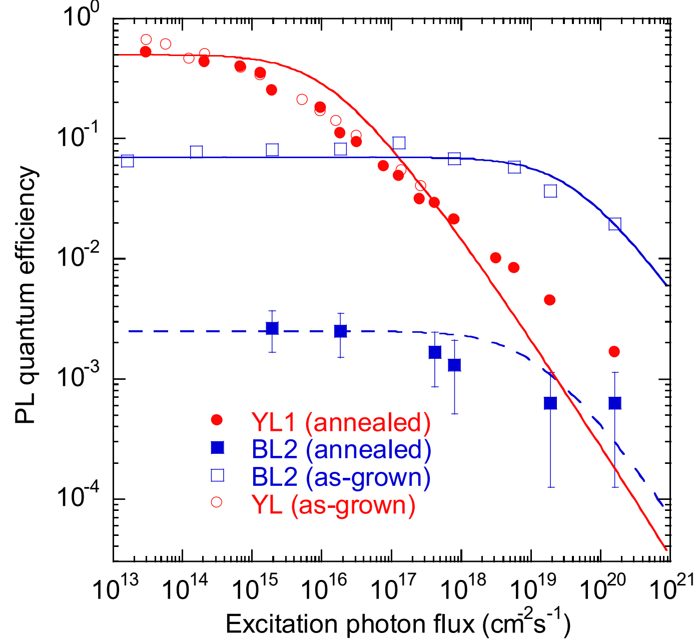

Fig. 13. The dependence of the PL quantum efficiency at T = 18 K on excitation intensity for as-grown GaN and GaN annealed in face-to-face geometry at T = 1050 °C (sample s1587). The lines are calculated using Eqs. (19) and (20) with the following parameters. η_{10} = 0.5, N_1 = 10^{17} cm^{-3}, τ_1^{lim} = 300 μs for the YL1 band, η_{20} = 0.07, N_2 = 5×10^{17} cm^{-3}, τ_2^{lim} = 0.3 μs for the BL2 band in as-grown GaN, and η_{20} = 0.0025, N_2 = 5×10^{14} cm^{-3}, τ_2^{lim} = 0.3 μs for the BL2 band after annealing at 1050 °C.

The parameters for the YL1 band obtained from fitting the excitation intensity dependence with Eq. (19) (given in the caption of Fig. 13) also have considerable uncertainty. Indeed, the YL1 band decays nonexponentially after a laser pulse at T = 18 K. It was assumed in the fit that N_{YL1} = 10^{17} cm^{-3}, and τ_i^{lim} = 300 μs. The latter value may be considered as the effective PL lifetime for the DAP-type transitions. The saturation of the YL1 efficiency begins at lower excitation intensities than the theoretical curve because of a longer lifetime for more distant pairs. The deviation at high excitation intensity can be explained by the increased contribution of close pairs, which are difficult to saturate because of their short lifetime. At room temperature, the YL1 decay becomes nearly exponential with the PL lifetime of about 50 μs.

More accurate estimates of the defect concentrations can be obtained by using Eq. (21) with $C_{p,\mathrm{BL2}}/C_{p,\mathrm{YL1}} = 0.12$ calculated in Sec. IVC. For sample s1587 with the total concentration of carbon $N_{\mathrm{BL2}} + N_{\mathrm{YL1}} = N_{\mathrm{C}} = 1.7\times10^{17}$ cm^{-3} found from the SIMS measurements, we estimate that $N_{\mathrm{BL2}} \approx 1\times10^{17}$ cm^{-3} (C_NH_i complexes) and $N_{\mathrm{YL1}} \approx 0.7\times10^{17}$ cm^{-3} (isolated C_N) in the as-grown sample before UV exposure.

V. SUMMARY

1. The BL2 band is caused by internal transitions of electrons from an excited state (~20 meV below the CBM) to the ground state (0.15 eV above the VBM) of the C_NH_i complex, which is a deep donor. A photogenerated hole is first captured at the ground 0/+ level of the C_NH_i defect. The excited hydrogenic state appears close to the conduction band when the defect is positively charged. This state quickly captures a free electron. The electron-hole recombination results in the BL2 band with the ZPL at 3.330 eV (in strain-free GaN), the band maximum at 3.0 eV, and the characteristic phonon structure on its high-energy side.
2. Under the above-bandgap illumination at $T \approx 20$ K, the C_NH_i complexes dissociate with probability $\gamma = 5\times10^{-8}$ in the process of electron-hole recombination via this defect. This results in the bleaching of the BL2 band and concurrent rise of the YL1 band associated with the isolated C_N defects. The dissociation is reversible so that after storing a sample for several hours at $T = 300$ K, the intensities of the YL1 and BL2 bands at $T = 20$ K partly restored to the original values (complete restoration is observed after approximately a month).
3. In the photo-induced dissociation process, the H component departs from the C_NH_i complex, overcomes a potential barrier with the height 1.3-1.9 eV, and becomes trapped in one of the near interstitial locations. The barrier for the complex restoration is 0.65-0.9 eV, and the complexes re-form after storing samples at room temperature for several hours.

4. The BL2 band disappears after the annealing at temperatures above 600 °C. The activation energy of this process is about 3.0 eV. This activation energy is obtained from Eq. (6), which accounts for the time of annealing. The BL2 band does not restore after several months of storing the annealed sample at room temperature. We conclude that the activation energy of 3 eV corresponds to the removal of hydrogen from the sample. The activation energies for the complex dissociation and diffusion of the H^+ ions are calculated to be much smaller (1.3 and 0.3 eV, respectively).

5. In the face-to-face annealing geometry (a GaN sample is covered with another one), the BL2 band disappears at significantly higher temperatures (above 1000 °C), which corresponds to an activation energy of 4.2 eV. We explain the increased barrier for the hydrogen removal by adsorption of the released hydrogen atoms by the top GaN layer and the exchange of H between the two layers.

6. The BL2 band in samples annealed at $T > 600$ °C can be restored by hydrogenation. Additional annealing of GaN at 850 °C in the N_2+H_2 ambient causes almost complete restoration of the BL2 intensity. Thus, annealing in the hydrogen-containing ambient introduces hydrogen to GaN, and the C_NH_i complexes are formed with concentrations comparable to the C_N concentration.

7. The C_NH_i donors capture holes efficiently with the hole-capture coefficient $C_{p,BL2} \approx 4.4\times10^{-8}$ cm^3/s. This agrees with the result of first-principles calculations that there is no barrier for the hole capture by a neutral C_NH_i complex. The knowledge of the hole-capture coefficients for the C_NH_i donors and C_N acceptors ($C_{p,YL1} = 3.7\times10^{-7}$ cm^3/s) allows us to find relative concentrations of these defects in GaN. To find the absolute concentration of one or both defects,

PL's excitation intensity dependence should be studied, and the absolute internal quantum efficiency for at least one PL band be found.

8. Finally, the BL2 band is quenched by the tunable (but not abrupt) mechanism, differently from the Schön-Klasens and Seitz-Mott mechanisms. The activation energy of the quenching is about 165 meV, which corresponds to the thermal emission of holes from the 0/+ level of the C_NH_i to the valence band. The critical temperature at which the quenching begins increases with increasing excitation intensity.

Acknowledgments

The work was supported by the National Science Foundation (grant DMR-1904861) and by the VCU PeRQ award. The calculations were performed at the VCU Center for High Performance Computing.

Data Availability

The data that support the findings of this study are available from the corresponding author upon reasonable request.

References

[1] M. A. Reshchikov, “Measurement and analysis of photoluminescence in GaN”, J. Appl. Phys. **129**, 121101 (2021).

[2] D. O. Demchenko, I. C. Diallo, and M. A. Reshchikov, “Hydrogen-carbon complexes and the blue luminescence band in GaN”, J. Appl. Phys. **119**, 035702 (2016).

[3] M. A. Reshchikov, M. Vorobiov, D. O. Demchenko, Ü. Özgür, H. Morkoç, A. Lesnik, M. P. Hoffmann, F. Hörich, A. Dadgar, and A. Strittmatter, “Two charge states of the C_N acceptor in GaN: Evidence from photoluminescence”, Phys. Rev. B **98**, 125207 (2018).

[4] S. Wu, X. Yang, Q. Zhang, Q. Shang, H. Huang, J. Shen, X. He, F. Xu, X. Wang, W. Ge, and B. Chen, “Direct evidence of hydrogen interaction with carbon: C-H complex in semi-insulating GaN”, Appl. Phys. Lett. **116**, 262101 (2020).

[5] G.-C. Yi and B. W. Wessels, “Carbon-hydrogen complexes in vapor phase epitaxial GaN”, Appl. Phys. Lett. **70**, 357-359 (1997).

[6] S. J. Pearton, J. C. Zolper, R. J. Shul, and F. Ren, “GaN: Processing, defects, and devices”, J. Appl. Phys. **86**, 1-78 (1999)

[7] S. Nakamura, T. Mukai, M. Senoh, and N. Iwasa, “Thermal annealing effects on p-type Mg-doped GaN films”, Jpn. J. Appl. Phys. **31**, Pt. 2, L139-L142 (1992).

[8] S. Nakamura, N. Iwasa, M. Senoh, and T. Mukai, “Hole compensation mechanism of p-type GaN films”, Jpn. J. Appl. Phys. **31**, Pt. 2, 1258-1266 (1992).

[9] M. S. Brandt, N. M. Johnson, R. J. Molnar, R. Singh, and T. D. Moustakas, “Hydrogenation of p-type gallium nitride”, Appl. Phys. Lett. **64**, 2264-2266 (1994).

[10] W. Gotz, N. M. Johnson, J. Walker, D. P. Bour, and R. A. Street, “Hydrogen passivation of Mg acceptors in GaN grown by metalorganic chemical vapor deposition”, Appl. Phys. Lett. **67**, 2666-2668 (1995).

[11] W. Gotz, N. M. Johnson, J. Walker, D. P. Bour, and R. A. Street, “Activation of acceptors in Mg-doped GaN grown by metalorganic chemical vapor deposition”, Appl. Phys. Lett. **68**, 667-669 (1996).

[12] S. J. Pearton, S. Bendi, K. S. Jones, V. Krishnamoorthy, R. G. Wilson, F. Ren, R. F. Karlicek, Jr., and R. A. Stall, "Reactivation of acceptors and trapping of hydrogen in GaN/InGaN double heterostructures", Appl. Phys. Lett. **69**, 1879-1881 (1996).

[13] R. Czernecki, E. Grzanka, R. Jakiela, S. Grzanka, C. Skierbiszewski, H. Turski, P. Perlin, T. Suski, K. Donimirski, and M. Leszczynski, "Hydrogen diffusion in GaN:Mg and GaN:Si", J. Alloys and Compounds **747**, 354-358 (2018).

[14] S. Limpijumnong and C. G. Van de Walle, "Stability, diffusivity, and vibrational properties of monoatomic and molecular hydrogen in wurtzite GaN", Phys. Rev. B **68**, 235203 (2003).

[15] J.-S. Park and K. J. Chang, "Diffusion and stability of hydrogen in Mg-doped GaN: A density functional study", Appl. Phys. Express **5**, 065601 (2012).

[16] S. M. Myers, A. F. Wright, G. A. Petersen, W. R. Wampler, C. H. Seager, M. H. Crawford, and J. Han, "Diffusion, release, and uptake of hydrogen in magnesium-doped gallium nitride: Theory and experiment", J. Appl. Phys. **89**, 3195-3202 (2001).

[17] J. Heyd, G. E. Scuseria, and M. Ernzerhof, "Hybrid functionals based on a screened Coulomb potential", J. Chem. Phys. **118**, 8207 (2003).

[18] D. O. Demchenko and M. A. Reshchikov, "Koopmans' tuning of HSE hybrid density functional for calculations of defects in semiconductors: A case study of carbon acceptor in GaN, J. Appl. Phys. **127**, 155701 (2020).

[19] C. Freysoldt, B. Grabowski, T. Hickel, J. Neugebauer, G. Kresse, A. Janotti, and C. G. Van de Walle, "First-principles calculations for point defects in solids", Rev. Mod. Phys. **86**, 253-305 (2014).

[20] C. Freysoldt, J. Neugebauer, and C. G. Van de Walle, "Fully *Ab Initio* Finite-Size Corrections for Charged-Defect Supercell Calculations", Phys. Rev. Lett. **102**, 016402 (2009).

[21] C. Freysoldt, J. Neugebauer, and C. G.Van de Walle, "Electrostatic interactions between charged defects in supercells", Phys. Stat. Sol. (b) **248**, 1067-1076 (2011).

[22] J. Neugebauer and C. G. Van de Walle, "Hydrogen in GaN: Novel aspects of common impurity", Phys. Rev. Lett. **75**, 4452-4456 (1995).

[23] J. L. Lyons, A. Janotti, and C. G. Van de Walle, "Carbon impurities and the yellow luminescence in GaN", Appl. Phys. Lett. **97**, 152108 (2010).

[24] M. A. Reshchikov, J. D. McNamara, F. Zhang, M. Monavarian, A. Usikov, H. Helava, Yu. Makarov, and H. Morkoç, "Zero-phonon line and fine structure of the yellow luminescence band in GaN", Phys. Rev. B **94**, 035201 (2016).

[25] J. L. Lyons, A. Janotti, and C. G. Van de Walle, "Effects of carbon on the electrical and optical properties of InN, GaN, and AlN", Phys. Rev. B **89**, 035204 (2014).

[26] M. Matsubara and E. Bellotti, "A first-principles study of carbon-related energy levels in GaN. I. Complexes formed by substitutional/interstitial carbons and gallium/nitrogen vacancies", J. Appl. Phys. **121**, 195701 (2017).

[27] T. Narita, K. Tomita, Y. Tokuda, T. Kogiso, M. Horita, and T. Kachi, "The origin of carbon-related carrier compensation in p-type GaN grown by MOVPE", J. Appl. Phys. **124**, 215701 (2018).

[28] W. Tang, E. Sanville, and G. Henkelman, **"**A grid-based Bader analysis algorithm without lattice bias", J. Phys.: Condens. Matter **21**, 084204 (2009).

[29] M. A. Reshchikov and R. Y. Korotkov, "Analysis of the temperature and excitation intensity dependencies of photoluminescence in undoped GaN films", Phys. Rev. B **64**, 115205 (2001).

[30] M. A. Reshchikov, A. A. Kvasov, M. F. Bishop, T. McMullen, A. Usikov, V. Soukhoveev, and V. A. Dmitriev, "Tunable and abrupt thermal quenching of photoluminescence in high-resistivity Zn-doped GaN", Phys. Rev. B **84**, 075212 (2011).

[31] B. T. Kelly, *Irradiation damage to solids*, Pergamon Press, London, 1966.

[32] K. L. Brower, "Dissociation kinetics of hydrogen-passivated (111) Si-SiO_2 interface defects", Phys. Rev. B **42**, 3444-3453 (1990).

[33] S. G. Koch, E. V. Lavrov, and J. Weber, "Towards understanding the hydrogen molecule in ZnO", Phys. Rev. B **90**, 205212 (2014).

[34] F. Tuomisto, V. Ranki, D. C. Look, and G. C. Farlow, "Introduction and recovery of Ga and N sublattice defects in electron-irradiated GaN", Phys. Rev. B **76**, 165207 (2007).

---

[35] M. A. Reshchikov and H. Morkoc, “Luminescence properties of defects in GaN”, J. Appl. Phys. **97**, 061301 (2005).

[36] M. A. Reshchikov, D. O. Demchenko, J. D. McNamara, S. Fernández-Garrido, and R. Calarco, “Green luminescence in Mg-doped GaN”, Phys. Rev. B **90**, 035207 (2014).

[37] M. A. Reshchikov, P. Ghimire, and D. O. Demchenko, “Magnesium acceptor in gallium nitride: I. Photoluminescence from Mg-doped GaN”, Phys. Rev. B **97**, 205204 (2018).

[38] M. A. Reshchikov, “Mechanisms of thermal quenching of defect-related luminescence in semiconductors”, Phys. Stat. Sol. A 2000101 (2020).

[39] M. A. Reshchikov, A. Usikov, H. Helava, Yu. Makarov, V. Prozheeva, I. Makkonen, F. Tuomisto, J. H. Leach, and K. Udwary, “Evaluation of the concentration of point defects in GaN”, Scientific Reports **7**, 9297 (2017).

[40] M. A. Reshchikov, Y. T. Moon, and H. Morkoç, “Origin of unstable photoluminescence in GaN: metastable defects or surface states?”, Phys. Stat. Sol. (c) **2**, 2716-2719 (2005).

[41] M. A. Reshchikov, “Determination of acceptor concentration in GaN from photoluminescence”, Appl. Phys. Lett. **88**, 202104 (2006).